

Chapter 1

Introduction

1.1 Background

In recent years, polycrystalline silicon thin-film transistors (poly-Si TFTs) become much more applicable in active matrix liquid crystal displays (AMLCDs)[1]-[3]. The applications of poly-Si TFTs on some memory devices such as static random access memories (SRAMs)[4], dynamic random access memories (DRAMs)[5], electrical programming read only memories (EPROMs)[6], electrical erasable programming read only memories (EEPROMs)[7] are also worthy to be studied. Poly-Si TFTs are also very potential to be used on devices such as linear image sensors [8], thermal printer heads [9], photodetector amplifier [10], scanner [11], neural networks [11], and three dimension LSIs [12].

In direct-view flat-panel displays, amorphous silicon (a-Si) TFTs has been commercially used in large area LCDs as the pixel switch. However, the external peripheral driving circuits must be connected to the pixel array. This increases the assembly complexity and cost especially at high-resolution displays. For poly-Si TFTs, it is easy to require mobility larger $50 \text{ cm}^2/Vs$, which is enough to be used as peripheral driving circuits [13]. Therefore, the pixel array and driving circuits can be made on the same glass. Such a monolithic display technology will dramatically reduce the assembly complexity and cost.

When comparing poly-Si film devices with single crystal devices, the differences of characteristics are mostly due to the presence of grain in poly-Si films. It is well known that there are lots of traps located in the grain boundary. These traps will trap carriers to form local depletion regions and construct potential barriers at grain

boundaries. Thus, the presence of grain boundary lowers carrier mobility and deteriorates device performance.

The characteristics of poly-Si TFTs can be improved when the channel dimensions are scaling down. However, the presence of grain boundaries in the poly-Si cause poly-Si TFTs to behave differently from their counterparts fabricated on single-crystal silicon substrate as the channel length becoming small. For instance, the threshold voltage lowering with decreasing gate length is more pronounced and behaves quite differently in poly-Si TFTs. The subthreshold swing becomes significantly sharp. Besides, shrinking down channel dimension might cause the characteristics variation of poly-Si TFTs due to the variation of the number of grain boundaries within the channel.

1. 2 Overview of grain control technologies

Many efforts have been given on the laser induced lateral grain growth of Si film for LTPS-TFTs, due to its higher mobility and better electrical uniformity, and so on. The former makes possible the SOP (system on panel) and the latter makes possible to use fewer TFTs to drive a pixel in organic EL displays. As for the occurrence of lateral growth, many bright methods have been proposed and realized, for example, SLS [14], PMELA (phase modulated excimer laser annealing)[15], CLC (continuous wave laser crystallization) [16]and so on. Although TFTs with mobilities with larger than $400\text{cm}^2/\text{Vs}$ have been achieved by these methods, but there are shortages that foregone 1st generation ELA system can not be applied for ELA processes due to additional complicated optical systems for laser light modification are necessary in these methods. $\mu\text{-Cz}$ [17]and Si film with selective floating structure[18] are also skillful methods where 1st generation ELA system is applicable, however, the film preparing processes are complicated. Meanwhile a new method for spontaneous lateral growth

of Si film was proposed and realized, and are called HREC (Heat retaining enhanced crystallization) method [19]. In this method active islands of TFT were pre-patterned and then were capped with a photosensitive film in previous to the laser annealing process.

1.3 Introduction of diamond like carbon (DLC)

Carbon usually exists in several forms; graphite, diamond, and the new form of fullerenes. All three of these forms are crystalline in structure but have varying properties based on the bonding order of the carbon atoms. Diamond-like carbon (DLC), on the other hand, is amorphous in structure, containing both sp^2 and sp^3 bonded carbon. As such, DLC has both diamond-like and graphitic properties. Hence the name diamond-like carbon (DLC).

DLC is used as LC alignment layer, passivation layer for machine and low-k and interlayer dielectric films in the IC. Now it is discovered that the DLC film shows good optical absorbance over a wide wavelength. So the DLC films can also be a good candidate to heat retaining layer.

1.4 Laser crystallization mechanisms

In laser crystallization technology, films are melted by laser irradiation and the nucleation happens at the cooler region. After laser irradiating, temperature gradient is formed. Heat flow sinks into the cooler region and the grain growth in the opposite direction. Then the growing grains meet and the grain boundary is formed. In many grain control technologies, the main idea is to control the heat gradient distribution. And if the cooling time of the whole film is extended, the nucleation seeds decrease and then grains grow larger. The simple schematic diagram of the melted silicon flow is showed in Fig.1-4-1.

1.5 Grain barrier carrier transport mechanism under high lateral field in poly-Si TFTs

The poly-Si material is, as previously mentioned, a heterogeneous material due to the presence of grain boundaries. These grain boundaries act as energy barriers that the carriers have to overcome. To describe the transportation in the polycrystalline material, the first point is to calculate the energy barrier present at grain boundaries, which limits the transport of carriers from one crystallite to the other. J.Y. Seto proposed the first credible model.[20]

1.5.1 Seto's model

The Seto's model is based on the following assumptions:

- Poly-Si film has small grain size, cubic shape.
- The single crystalline silicon energy band structure is assumed to be applicable inside the crystallites,
- Doping concentration in poly-Si is uniform,
- All the doping atoms are ionized,
- All the grains have the same size, cubic shape,
- The representation is mono-dimensional,
- The grain boundaries have no thickness,
- The defects are carrier traps that are located in the grain boundaries. In this condition, the trap concentration is defined per surface unit. The trap is assumed to be initially neutral and become charged by trapping carriers,
- The traps are acceptors in the n-type and donors in the p-typed semiconductor,
- The trap energy level is unique and located more or less in middle of the forbidden band.

Barrier height calculation:

We consider the different following parameters: X , extension of the space charge region; N_D , donor doping atom concentration; N_{TA} , acceptor like trap surface density at grain boundaries; ε_0 , permittivity in vacuum; ε_s , semiconductor permittivity; L_G , size of the grain; φ , the electrostatic potential; x , the position coordinate.

The distribution of the charges in the material is schematically described Fig.1-5-1. At grain boundaries, the surface trap charge density is qN_{TA} , which thus compensates the charge of the volume ionized doping atom concentration (qN_D). An abrupt depletion approximation is used to calculate the energy band diagram in the crystallite.

$$\text{In the space charge region, for } 0 < x < \frac{X}{2} \quad \frac{d^2 \varphi}{dx^2} = \frac{qN_D}{\varepsilon_s \varepsilon_0} \quad (1-5-1)$$

$$\text{Out of the space charge region, } \frac{X}{2} < x < \frac{L_G}{2} \quad \frac{d^2 \varphi}{dx^2} = 0 \quad (1-5-2)$$

Considering that at the border of the space charge region the electric field is null:

$$\left[\frac{d\varphi}{dx} \right]_{x=X/2} = 0 \text{ for } 0 < x < \frac{X}{2} : \frac{d\varphi}{dx} = \frac{qN_D}{\varepsilon_s \varepsilon_0} x + cst = \frac{qN_D}{\varepsilon_s \varepsilon_0} \left(\frac{X}{2} - x \right)$$

$$\frac{X}{2} < x < \frac{L_G}{2} : \varphi(x) = \varphi\left(\frac{X}{2}\right) : \varphi(x) = \frac{qN_D}{2\varepsilon_s \varepsilon_0} \left(\frac{X}{2} - x \right)^2 + \varphi\left(\frac{X}{2}\right)$$

Thus the energy barrier height (E_B) is defined at grain boundaries as the energy difference between the positions $x = 0$ and $x = \frac{X}{2}$.

$$E_B = - \left(q\varphi(0) - q\varphi\left(\frac{X}{2}\right) \right) = + \frac{q^2 N_D}{2\varepsilon_s \varepsilon_0} \left(\frac{X}{2} \right)^2 \quad E_B = + \frac{q^2 N_D}{8\varepsilon_s \varepsilon_0} X^2 \quad (1-5-3)$$

The value of X has to verify for the electrical neutrality of the global material, which means $XqN_D^+ = qN_{TA}^-$. N_{TA}^- is the ionized part of N_{TA} .

The Seto's model defines a critical concentration (N_D^*), which corresponds to this

$$\text{limit: } \frac{X}{2} = \frac{L_G}{2} \rightarrow X = L_G \rightarrow N_D^* = \frac{N_{TA}}{L_G} \quad (1-5-4)$$

For a fixed trap density, if the effective doping concentration is higher than the critical concentration, the space charge extension is lower than the crystallite size. On the contrary, the crystallite is fully depleted.

$$N_D > N_D^* : X = \frac{N_{TA}}{N_D} \quad \text{and} \quad E_B = + \frac{q^2 N_{TA}^2}{8 \epsilon_s \epsilon_0 N_D} \quad (1-5-5)$$

The expressions of the potential in the both regions are shown as follows:

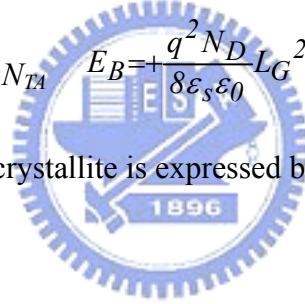
$$0 < x < \frac{X}{2} \quad \varphi(x) = - \frac{q N_D}{2 \epsilon_s \epsilon_0} \left(\frac{N_{TA}}{2 N_D} - x \right)^2 \quad (1-5-6)$$

$$\frac{X}{2} < x < \frac{L_G}{2} \quad \varphi(x) = 0 \quad (1-5-7)$$

$$N_D < N_D^* : X = L_G, \text{ with } L_G N_D = N_{TA} \quad E_B = + \frac{q^2 N_D L_G^2}{8 \epsilon_s \epsilon_0} \quad (1-5-8)$$

The potential variation in the crystallite is expressed by the following:

$$\varphi(x) = - \frac{q N_D}{2 \epsilon_s \epsilon_0} \left(\frac{L_G}{2} - x \right)^2$$



In intrinsic semiconductor, the effective doping concentration N_{eff} is controlled by the gate voltage. Therefore the relationship between energy barrier height and gate voltage is showed in Fig.1-5-2.

1.5.2 Possible grain boundary carrier transport mechanism in poly-Si TFTs

These are many possible transport mechanisms of carrier through the grain boundary energy barrier. Which one is the most powerful reason for kink effect in poly-Si? It is discussed as follows:

Grain boundary barrier scattering

The carrier transport mechanism through the grain boundary is scattered by grain boundary because of the existence of grain boundary energy barrier. Carriers pass

through the grain boundary should overcome the grain boundary energy barrier. As a result, when the grain boundary barrier height decreases, the carrier transport through the grain boundary becomes easier. And this non-scattered carrier with high energy can act as an avalanche multiplication source. Therefore, when the grain boundary decreases, the kink effect becomes serious.

In Fig.1-5-3, the output characteristic of device before and after passivation is showed. After passivation, the trap state of the poly-Si film is repaired, and the grain boundary barrier height is reduced. It is found that after passivation, the kink effect is suppressed. This result does not correspond to the mechanism proposed above. So the grain boundary scattering effect is not the right mechanism of kink effect in poly-Si TFTs.

Impact ionization by lucky electron

In the lucky electron model, it is not the carriers with the average energy that can initialize impact ionization, but only those larger than an energy threshold energy E_{th} . The original of these high-energy carriers is from a “lucky” population of electrons which go without scattering for a distance x , much larger than the mean free path of collision λ . The distance x that an electron has to travel to gain this amount of the kinetic energy from the potential energy is:

$$q = E_x = qE_{th} \Rightarrow x = \frac{E_{th}}{E} \quad (1-5-14)$$

The concentration n of these lucky electrons is:

$$n = n_0 \exp\left(\frac{-E_{th}}{E\lambda}\right) \quad (1-5-15)$$

The impact ionization coefficient α is:

$$\alpha \propto n = n_0 \exp\left(\frac{-E_{th}}{E\lambda}\right) \quad (1-5-16)$$

Thus, the measured ionization rates are often expressed in the empirical form of

$$\alpha = A_i \exp\left(\frac{-\beta}{E}\right) \quad (\#/cm); \quad \beta = \frac{E_{th}}{\lambda} \quad (1-5-17)$$

The excess kink current of polysilicon TFTs can be given by

$$I_{kink} = I_{DIGBL} \int_0^{\Delta L} A_i \exp\left(\frac{-\beta}{E}\right) dx \quad (1-5-18)$$

Replacing dx by $\frac{dx}{dE} dE = -E^2 \frac{dx}{dE} d\left(\frac{1}{E}\right)$ and $\frac{dE}{dx} = \frac{E}{l}$ we have

$$I_{kink} = -I_{DIGBL} \int_{E_{source}}^{E_m} A_i \exp\left(\frac{-\beta}{E}\right) l E d\left(\frac{1}{E}\right) \quad (1-5-19)$$

Since the $\exp(-\beta/E)$ is the most dominated function of E , thus we may replacing E in the other mildly variation terms with E_m . That is replacing lE by lE_m .

The excess kink current becomes

$$I_{kink} = I_{DIGBL} \int_{E_{source}}^{E_m} A_i \exp\left(\frac{-\beta}{E}\right) l E_m d\left(\frac{1}{E}\right) \quad (1-5-20)$$

$$\Rightarrow I_{kink} = \frac{A_i}{\beta} l E_m \exp\left(\frac{-\beta}{E_m}\right) \times I_{DIGBL} \quad (1-5-21)$$

The maximum electric field can be replaced by

$$E_m = \sqrt{\frac{V_{ds} - V_{dsat}}{l} + E_{sat}^2} \cong \frac{V_{ds} - V_{dsat}}{l} \quad (\text{if } \frac{V_{ds} - V_{dsat}}{l} \gg E_{sat}) \quad (1-5-22)$$

$$\Rightarrow I_{kink} = \frac{A_i}{\beta} (V_{ds} - V_{dsat}) \exp\left(\frac{-\beta l}{V_{ds} - V_{dsat}}\right) \times I_{DIGBL} \quad (1-5-23)$$

Thus the multiplication factor M is defined by I_{kink}/I_{DIGBL} :

$$M = \frac{I_{kink}}{I_{DIGBL}} = \frac{A_i}{\beta} (V_{ds} - V_{dsat}) \exp\left(\frac{-\beta l}{V_{ds} - V_{dsat}}\right) \quad (1-5-24)$$

<Threshold energy>

Since these density of states may act as a generation center in the impact ionization process. Only the acceptor-like traps are considered in the derivation since our samples are n-type polysilicon thin film transistors.

The acceptor-like trap that under the quasi-Fermi level is negative charged. One high energy electron can knock and electron out at this trap state and the “activation

energy” is from this charged trap energy level to the conduction band edge, as shown in Fig.1-5-4. Thus, the energy and momentum conservation relation is given as:

$$\frac{1}{2}m_eV_1^2 = (E_g - E_T) + 2 \times \frac{1}{2}m_eV_2^2$$

and

$$m_eV_1 = 2m_eV_2$$

By solving the above two equations the threshold energy distribution in the band gap can be obtained as

$$E_{th}(E_T) = 2(E_g - E_T)$$

Consequently, the threshold energy that we adopt into the Shockley’s “lucky electron model” is E_{th} .

For the same crystallize poly-Si film, when the gate voltage increases, the Fermi lift up. And the threshold energy E_{th} becomes smaller. By the equation derived above, when the threshold energy decreases, the multiplication factor becomes larger. It means that increasing the gate bias will enlarge the kink effect. This also does not correspond to our experimental results.

We will propose a new reason of grain boundary carrier transport mechanism under high lateral electric field in Chapter3.

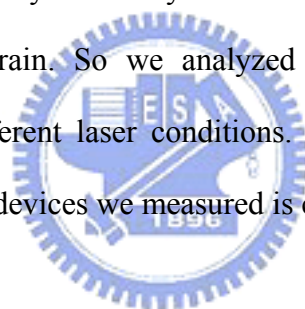
1.6 Motivation

The laser crystallization technologies by excimer laser have been extensively studied. But when the laser crystallization technologies are applied to the large size glass substrate, the issue of uniformity becomes important. In excimer laser, the relation between grain size and laser energy density are showed in Fig.1-6-1. It is found that the fine grain appears right after the best condition. And the grain size changes rapidly before the best condition. These result in narrow process window. If

we care about the issue of uniformity, the performance should be sacrificed. The grain control technology is introduced to solve these problems above. When the grain growth position and grain qualities are controlled, the uniformity performance of devices can be achieved. There are many methods can realize this uniformity request. We chose one of these technologies—heat retaining enhanced crystallization (H-REC), because of its simple fabrication process.

As to the novel laser instruments appear. The traditional heat retaining material is not suitable for the long wavelength laser. So we introduced a new heat retaining material and applied it into the H-REC experiment.

Then we discovered that the grain affect on the high electric field effect: “Kink effect”. And kink effect is mainly caused by the avalanche multiplication factor in the depletion region near the drain. So we analyzed the multiplication factor with different bias and under different laser conditions. To study the kink effect more clearly, the channel length of devices we measured is chosen to be short.



1.7 Thesis outline

This thesis is divided into two parts. The first one is the grain control experimental. Second, the grain influence of kink effect is also studied. In our grain control technology, short channel devices can be fabricated on our grain controlled film. Furthermore, short channel devices often suffer from serious kink effect. However, the kink effect affected by grain is not studied. So we analyze the grain influence on kink effect.

In chapter 1, we describe many technologies of grain control and introduce the new material we used in our experiment. Then some possible reason for kink effect in polysilicon TFTs are proposed. The model of the grain boundary barrier height (E_B) which plays an important role in our kink effect analysis is briefly showed.

In chapter 2, the material analysis and experimental instruments are described. The deposition condition and the material basic properties are also mentioned in this chapter. And the results of DLC heat retaining enhanced crystallization with different laser energy density ($400mJ/cm^2$ - $600mJ/cm^2$) and different sample structure are proposed.

In chapter 3, first, we introduce the parameters extraction methods of kink effect analysis. In our parameter extraction, we also contain a simple method to rectify the anomalous drain current caused by channel length modulation. Then we investigate a new grain influenced mechanism of kink effect in polysilicon TFTs. The data analysis of different bias and different laser condition are also showed.

In chapter 4, the conclusions of our experiments are showed.



Chapter 2

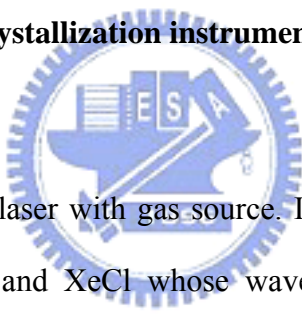
Experimental and Material Analysis

2.1 Instrument

In this section, we would introduce the laser instrument used to crystallize the a-Si and the material analysis instrument—Raman spectroscopy which is used to obtain nondestructive characterization of the crystallinity and stress in poly-Silicon films.

2.1.1 Introduction of laser crystallization instrument

A. Excimer laser



Excimer laser is a pulse laser with gas source. In our experiment there are two kinds of laser sources: XeF and XeCl whose wave length is $351nm$ and $308nm$ respectively. A-Si exhibits higher absorption of excimer laser than solid state green laser. As to the XeCl excimer laser the pulse frequency is $300Hz$ and the beam size is $300m \times 0.4mm$. The profile of beam is flat top type. Finally, the maximum output power is $1Joule$.

B. Solid state green laser

Solid sate laser is a high power pulse laser with solid phase laser source which introduce more stable laser power and lower maintenance fee than conventional exceimer laser. This green laser is produced by second harmonics of Nd:YAG and its wave length is $532nm$. The size of laser is $105mm \times 40um$ and the maximum laser power is $200W$. Frequency of laser irradiation is $4000Hz$.

2.1.2 Introduction of Raman

Raman spectroscopy can show the crystallinity of films. And it is useful for nondestructive characterization of stress and defects in poly-Si films. The single crystal silicon optical phonon mode exhibits a line at 520.8cm^{-1} in the Raman spectra. Its peak frequency and full width at half-maximum (FWHM) are sensitive to stress, defects and grain size. For large grains, the peak position is determined by tensile stress and FWHM was related to defects. When the peak position comes close to the single crystal at 520.8cm^{-1} , the film quality is getting better. The FWHM of Si wafer is 4.4cm^{-1} . When the value of FWHM comes close to 4.4cm^{-1} , the crystallinity is improved.

2.2 Diamond like carbon characteristics

2.2.1 Diamond like carbon deposition

Diamond like carbon (DLC) is deposited by plasma-enhanced chemical vapor deposition (PECVD) under the RF power of 100W for 45 minute. The DLC film is formed by hydrogen (H_2) and methane (CH_4) of the flow rate: 10.3sccm with the ratio of 1:1 under the pressure of 18mtorr . The deposition rate of DLC films is about 130nm/hr .

2.2.2 Material analysis:

Light transmission and reflection

In heat retaining enhanced crystallization technology, SiO_xN_y is a more mature material than DLC. But why we choose DLC film instead of the SiO_xN_y ? Because the novel laser instruments which is widely-researched recently turn the laser wavelength

into the one far away from the UV light region. The transmittance at 532nm of 150nm thick SiO_x and SiO_xN_y is 99.66% and 94.7% individually. Though the transmittance of the SiO_x and SiO_xN_y which have been used as a heat retaining layer for a long time, we can see that the transmittance of these materials becomes near 100% with the laser wavelength coming closer to the infrared region.

The diamond like carbon (DLC) film is chosen to be our heat retaining layer. Because the DLC film exhibits strong optical absorption ability: low transmittance and low reflectivity of light in a wide range of wavelength. As a heat retaining layer, DLC film is suitable for any available laser instrument nowadays such as, excimer laser and solid state green laser.

The reflectivity and transitivity of DLC are measured by N&K and ultraviolet-visible (UV-VIS) spectrophotometer (Perkin Elmer Lambda 650) respectively. The result is showed in Fig.2-2-1 and Fig.2-2-2. We can find that the reflectivity of DLC at 532nm is 11.09% and the transmittance is 25.66%. These indicate that the DLC films have an optical absorbance up to 63.25%. As to the most popular XeCl excimer laser, the reflectivity and transmittance of DLC are 11.78% and 1.27% respectively. Thus DLC film also shows a strong superiority to be a candidate of heat retaining layer of excimer laser.

Raman spectroscopy

There are two important Raman peaks of DLC films: the D band at 1360 cm^{-1} associated with sp³-bond vibration (disorder) and the G band at 1590 cm^{-1} associated with disordered sp²-bond vibration (graphite) [21]. Fig.2-2-3 shows the Raman spectrum of DLC before and after laser irradiated. It is found that the DLC is crystallized after laser irradiated. But the crystallized DLC films can also be a heat retaining layer. After laser irradiated, the signal of disorder appears. But increasing the

laser energy, there is no significant change in the Raman spectra obtained by XeF excimer laser at $300\text{-}500\text{mJ/cm}^2$. From Fig.2-2-4 the calculated absorption of DLC increases with the laser energy density. It proves that the DLC film can also be a good heat retaining layer during laser irradiation. If the DLC film is over burned, the signal of the oxide under-layer will appear. However this situation does not appear during our laser experiment. This result suggests that the properties of the DLC film are negligibly changed upon rapid heating with the laser irradiation.

2.3 Amorphous silicon thin film with and without capped DLC crystallized by ELA

In this section, the laser we used is XeF excimer laser (351nm) with the laser energy density of $400\text{ to }600\text{mJ/cm}^2$.

2.3.1 Sample fabrication and Laser irradiation

Sample A

Sample A is prepared to directly study the influence of DLC. The cross-section of sample A is showed in Fig.2-3-1. The space (S_D) between DLC patterns are 3, 6, 10, 20, 30, 50, $60\mu\text{m}$ and the length (L_D) of DLC are 4, 6, 8, 12, 16, 20, 30, $60\mu\text{m}$. First, the buffer layer (SiN_x 500\AA / SiO_2 1000\AA) is deposited on the glass substrate, and then the 1000\AA thick amorphous silicon is also deposited subsequently. Finally, the DLC (1000\AA) film was capped on the silicon film and patterned by lift off method.

Sample B

Sample B is prepared to learn about the influence of pad oxide under DLC. Fig.2-3-2(a) shows the cross-section of sample B. The pad oxide layer (1000\AA) is deposited between the DLC and silicon films of sample A. The reference of sample B

without DLC capped is showed in Fig.2-3-2(b).

2.3.2 Material analysis:

Sample A

As we know, the DLC film has high optical absorption ability. So the amorphous silicon film under DLC pattern is greatly heated while the laser is irradiating. And then it keeps in higher temperature than the silicon film without DLC capped. Subsequently, a considerable lateral temperature gradient occurs near the DLC patterns and the lateral growth grain appears near the DLC pattern. However, the silicon film far from the DLC patterns is crystallized and becomes fine grain. In Fig. 2-3-3(a)-(c), we observed that there is a line in the middle of the DLC patterns with different laser energy density (from $400\text{mJ}/\text{cm}^2$ to $600\text{mJ}/\text{cm}^2$). Though the atomic force microscope (AFM) which is showed in Fig.2-3-4, we find that the line at the middle of the DLC patterns is where the local minimum appears. We think that the crystallization begins from the middle of the DLC patterns toward the boundary of the DLC patterns. But the heat from DLC is only sufficient to offer the heat of lateral grain growth near DLC. As to the a-Si films at the middle of DLC patterns, DLC also affect on them, but DLC can not offer enough heat to that long term.

Additionally, the surface of crystallized poly-silicon is very flat. As to the surface roughness measured by AFM is about 5.78nm , which is very similar to the surface roughness of poly-silicon irradiated by ELA without capping any DLC films (5.77nm). Fig.2-3-5 (a)-(c), the scanning electron microscope (SEM) results of sample A, show the grain size around DLC patterns after laser irradiated ($400\text{-}600\text{mJ}/\text{cm}^2$). The average grain size near the DLC patterns under laser energy density of $400\text{mJ}/\text{cm}^2$, $500\text{mJ}/\text{cm}^2$ and $600\text{mJ}/\text{cm}^2$ are $0.6\mu\text{m}$, $0.7\mu\text{m}$ and $1\mu\text{m}$ respectively. However the average grain size of the same laser energy density far from DLC films is about 60nm ,

75nm and 100nm individually. The result is an evident that the DLC enhanced grain size is about 10 times larger than the normal one and by the grain control technology of DLC enhanced method, the grain grows laterally. In the experiment have been done before [22], the lateral growth grain shows better electrical qualities in the thin film transistors.

By the way, the widest width between two DLC patterns is 60um, this situation suggested that the influence of DLC could reach a long-term distance but DLC dose not offer enough heat for the lateral grain growth, where far from the DLC pattern. It also confirmed by the Raman spectra. In Fig.2-3-6 the Raman spectra of different position between and far from the DLC patterns is showed and the laser energy density is 500mJ/cm². We can see that there is negligible change of Raman spectra of the peak position and the full width at half maximum (FWHM) between and far from two DLC patterns.

We also find a new nondestructive method to analyze the quality of crystallinity. The Raman spectra can offer a high speed and precise result of crystallization. The Raman spectra of the lateral grain near DLC patterns are showed in Fig.2-3-7(a)-(c), which irradiated by different laser energy density of 400-600mJ/cm². With the laser energy density increases, the peak position comes near to the single crystal position (520.8cm⁻¹) and the full width at half maximum (FWHM) decreases. It means that when the laser energy density increases, the crystallinity becomes better and these results agree with the observation from SEM.

Sample B

Carbon is a serious contamination of silicon. Therefore, the pad oxide is prepared between DLC and silicon films to block the contamination from DLC. Sample B is prepared to learn about the influence of pad oxide under DLC. The transmittance of

silicon oxide layer is almost 100% for the wavelength of 351nm excimer laser and the silicon oxide film have been used as an anti-reflection coating material. So the reflectivity and absorptivity of silicon oxide is very low. As a result, the pad oxide does not influence on the optical absorption. However, the thick pad oxide film will block the heat from the amorphous silicon film. The delivery of heat is degraded.

From the Raman analysis showed in Fig.2-3-8(a)-(b), it is found that the crystallinity is also improved by increasing the laser energy density. And we can see that from Fig.2-3-8 (c), the FWHM of reference sample without DLC patterns are bad. As to sample B, the FWHM value is obviously improved. However the FWHM value of sample B is larger than the value of sample A. FWHM value directly reflect the crystallinity of silicon films. Therefore, DLC pattern indeed improves the silicon film quality. But pad oxide layer degrades the crystallinity by blocking the heat delivery.

Compare sample A to sample B, the peak position of sample B is slightly worse than sample A. And the FWHM value of sample B is lager than sample A. Nevertheless, the quality of the crystallized silicon film is still good. Thus we can make a conclusion that the pad oxide layer slightly degrades the crystallinity, but still good. The DLC shows the ability of crystallization enhancement.

2.4 Crystallization mechanism for 1000A a-Si with heat retaining layer of DLC

Because the DLC film has higher optical absorbance, the DLC film will be heated to a higher temperature than amorphous silicon while the laser is irradiating. And the heating resistance of DLC is also very high, up to 5000K. So the DLC film is suitable for a heating source. We could define our active island right among the DLC

patterns, and then the DLC patterns would act as heating source. The heat flow moves downward to lower temperature and the grain growth happens in the opposite direction. So the lateral growth grain nucleation sites appear near the DLC patterns, and grow toward the DLC pattern. Amorphous silicon film located far from the DLC patterns crystallized as fine grain. The crystallinity is not degraded by DLC films. Because the Raman shift under the same laser energy density with and without DLC patterns is almost the same, which is about 516.2 cm^{-1} . During this experiment we use 351nm excimer laser, with one shot laser crystallization. Unlike the traditional ones, with 95% overlap laser crystallization, our laser beam is non-overlap. So the laser energy density would not influence on the heat gradient, it just acts as an energy supply. The heat gradient would form spontaneously by the design of DLC patterns. The schematic diagram of the proposed crystallization process is showed as Fig. 2-4-1.



Chapter 3

Analysis of Kink Effect in Poly-Si TFTs

3.1 Possible kink effect related mechanisms

As the poly-Si TFTs are operated at high drain bias, the output characteristics show an anomalous drain current increase or an increase of the out put conductance. We called this phenomenon the “kink effect”. This effect has been investigated extensively in single-crystal MOSFETs or SOI devices. In general, the kink effect involves many different physical mechanisms, such as (i) punch-through [23], (ii) drain induced barrier lowering (DIBL) [24], (iii) charge sharing effect [25], (iv) channel length modulation, (v) impact ionization or avalanche induced breakdown, (vi) body effect induced threshold voltage roll off, and (vii) parasitic BJT effect. Furthermore, for poly-Si TFTs, because of the presence of grain boundary, (viii) drain induced grain barrier lowering (DIGBL) and (ix) grain boundary trap-enhanced kink effect: a novel possible reason for kink effect, which is proposed by Dimitriadis et al [26].

3.2 Device fabrication

The Fig.3-2-1 shows that cross-sectional view of poly-Si TFT with self-align source/drain. These devices are fabricated as a conventional top-gate structure on glass substrate with the channel film thickness of $50nm$. The film is crystallized by solid state green laser (SSL) with different laser energy density vary from $369mJ/cm^2$ to $714mJ/cm^2$. And also one sample was crystallized by ELA ($308nm$) with its best laser condition. In our study, the amorphous silicon films is crystallized by different laser power energy and different laser sources are prepared to research into different

crystallization condition poly-Si TFTs. The channel width spreads from $1\mu m$ to $30\mu m$ and the channel length varies from $1\mu m$ to $30\mu m$.

From the SEM observation, we can find that, the grain size increases with the laser energy density. And the average grain size of different laser energy density and laser source is defined as Table I.

3.3 Parameter extracted method

Because of the absence of the substrate contact in TFT or SOI devices, a simple method to determine the kink current was adopted. This method can allow an easy and reasonable characteristic analysis of the kink effect.

In this study, the saturation voltage was extracted from the output conductance directly. Each saturation voltage at various gate voltages can be defined from the “first” minimum points of the conductance, as illustrated in Fig.3-3-1. Then, we could obtain the drain current that have not been triggered by multiplication effect from these saturation points. And then we could predict the non-saturate drain current trend caused by the channel length modulation and this rectified drain current is donated as $I_{D,SAT}$ here. As showed in Fig.3-3-2. Therefore, the kink current I_{KINK} can be evaluated by using the drain current at high drain voltage to minus the rectified saturation current triggered by the channel length modulation, such that $I_{KINK}=I_{DS}-I_{D,SAT}$ (Fig.3-3-2). If we normalized the kink current by the non kink effect triggered current, the total multiplication factor which involves the impact ionization effect and drain induced barrier lowering in the pinch-off region can be obtained, thus $M=I_{KINK}/I_{D,SAT}$.

The grain boundary barrier height is discussed in this chapter to represent the influence of electrical field at the grain boundary is extracted by the effective electrical activation energy at the grain boundary: E_B . The activation energy (E_B) of

the on current was obtained from the slope of Arrhenius plot (Fig.3-3-3) of drain current. The data which was taken over a temperature range from 25 °C to 100 °C follows a straight line. From the slope of this straight line, we could obtain the effective electric activation energy at the grain boundary E_B .

The trap density is extracted by the Levinsion proposed method from the slope of Fig.3-3-4. To make sure the trap density was fully occupied, the gate voltage is chosen from 6V to 10V.

3.4 Electrical characteristics

3.4.1 Different laser crystallized quality

The anomalous current increment in poly-Si TFTs called “kink effect” is mainly due to the avalanche multiplication in the depletion region near the drain. So we take the multiplication factor as a reference parameter to represent the influence of kink effect. We found that the kink effect is also affected by grain. Because the local maximum channel electric field (E_m) in poly-Si TFTs is strongly influenced by the grain boundaries. We believe that the local maximum electric field (E_m) occurs in the vicinity of the grain boundary because of the high electric energy trap at the grain boundary. As showed in Fig.3-4-1(a), carriers are accelerated by the grain boundary energy trap and generate electron-hole pairs by avalanche multiplication. Therefore when the grain barrier height increases, the local maximum electric field (E_m) in poly-Si film increases and then the kink effect becomes more serious. We assume that the poly-Si is fully depleted near the drain, and then the rate of voltage drop in the vicinity of the grain boundary is strong related to the grain size (L_G). So if we fix the grain boundary barrier height in poly-Si film, then when the grain size increases, the slope of voltage drop becomes gentle (Fig.3-4-1(b)). And the maximum electric field (E_m) becomes smaller. In conclusion, the avalanche multiplication increases with the

grain barrier height (E_B) increases and decreases with the grain size (L_G) increases.

First, we study the influence of E_B , from Fig 3-4-2(a), The grain boundary barrier height under laser energy density of $415mJ/cm^2$ is found that the grain boundary barrier height decreases rapidly with the gate voltage. And its multiplication factor also decreases rapidly with the gate voltage (Fig.3-4-2(b)). This result consistent with the concept we proposed above. Moreover, when the gate voltage is high, the grain boundary barrier height becomes small, and the value of E_B is negligible. Then the influence of phonon scattering appears. As a result, the multiplication factor (M) becomes saturate and the value is quite small under high gate voltage. Fig. 3-4-3 and Fig.3-4-4 show the E_B and M versus gate voltage under different laser energy density. We can see that with different laser energy density, the behavior is the same.

Second, the influence of grain size is studied. Fig.3-4-5 shows the trap density of SSL with different grain sizes. It is found that when the grain size increases from $0.3\mu m$ to $1\mu m$, the trap density is almost the same. So all the analysis below, we choose the film crystallized by SSL with grain sizes vary from $0.3\mu m$ to $1\mu m$ (laser energy density from $415mJ/cm^2$ to $507mJ/cm^2$) and the grain boundary barrier height is set the same. From Fig.3-4-6, the figures of multiplication factors with different laser energy density are normalized to the same scale. And it is found that the multiplication factor indeed decreases with the laser energy density enlarging. This result is also consistent with our proposed concept. Moreover, when the laser energy density increases, the grain size increases. Following the conception proposed above, while the laser energy density increases, the maximum electric field (E_m) becomes smaller. A lower E_m leads to a smaller multiplication factor (M). In conclusion, kink effect is mainly affected by (i) the grain barrier height and (ii) grain size. So enlarging the grain size could suppress avalanche multiplication.

3.4.2 Different bias voltage

It is known that the increase of drain voltage cause serious kink effect. When the drain voltage increases, the lateral electric field becomes larger. Thus the electron is accelerated by (i) drain bias (ii) grain boundary energy drop (Fig.3-4-7). Therefore the value of E_m increases with the drain voltage and the multiplication factor M also increases with the drain voltage (Fig.3-4-8). Different laser energy density films show the same thing.

For a constant drain voltage, as the gate voltage increases, M decreases due to (i) reduction of the effective lateral electric field (ii) decrease of the effective grain barrier height. When the gate voltage increases, kink effect is suppressed.

Since the acceleration source of drain is suppressed. Furthermore while the gate voltage is rising, the gate induced carrier filled the trap of the grain boundary. And then the effective grain barrier height reduces. Thus the multiplication factor decreases as the gate voltage increases (Fig.3-4-9).

When the gate voltage is high, the grain boundary barrier height becomes small. Then the influence of phonon scattering appears. It is also observed that the grain boundary barrier height of a high gate voltage can be neglect because of its small value. It is found that the larger the laser energy density is, the faster the value of M is negligible. It is showed in Fig.3-4-10. It is known that devices with better quality silicon active layer suffer from phonon scattering caused by gate voltage easier. Thus it is found that while the grain size enlarging, the multiplication factor (M) decreases faster with the gate voltage increases.

3.4.3 Different laser crystallization

Form Table I, we can see that the average grain size of ELA ($380mJ/cm^2$) is similar to SSL $415mJ/cm^2$. However because of the difference of laser crystallization

mechanism between ELA and SSL, the grain boundary quality of each laser instrument is different. Fig. 3-4-11 shows the grain barrier height of ELA and SSL $415mJ/cm^2$ crystallized silicon films. It is showed that the grain barrier height of ELA is larger than the SSL $415mJ/cm^2$ one. According to the grain boundary enhanced kink effect mechanism, under high lateral electric field, the multiplication factor of ELA is larger than the one of SSL $415mJ/cm^2$. As showed in Fig.3-4-12.

Comparing ELA with SSL, the grain boundary quality of SSL is better than ELA's (Fig.3-4-13). Moreover, the grain size of SSL with laser energy density more than $415mJ/cm^2$ is larger than the one of ELA. In conclusion, the kink effect is less serious in SSL films than ELA's. As showed in Fig.3-4-14. SSL can enlarging the grain size and also improve the grain boundary quality at the same time.

Table II shows the trap density of ELA and SSL with laser energy density of $415mJ/cm^2$ to $507mJ/cm^2$. It is found that the trap density of ELA is lager than SSL with laser energy density lager than $415mJ/cm^2$. The larger the trap density is the lager the multiplication factor is. It is also consistent with our experimental results.

3.4.4 Kink current

Kink current is defined as: $I_{KINK}-I_{D,SAT}'$. $I_{D,SAT}'$ include the effect of channel length modulation. Getting rid of channel modulation, the kink effect can be analyzed more purely. In Fig.3-4-15, it is discovered that the kink current is initially increases with the gate voltage and starts to decrease at high gate voltage after peaking. The initial increase of the kink current is due to the increase of the gate-induced electrons, whereas the decrease at higher gate voltages is due to the vertical field scattering caused by gate voltage. And this phonon scattering happens in devices with quality silicon films easier. Therefore the positions of peak appearance decrease with the laser energy density increases. Also the kink current is larger when the drain bias is

larger. Since under higher lateral electric field, kink current generated more.

As we know, under the same laser instrument when the grain size increases, the drain current increases. The avalanche multiplication is dominated by the electric field, but the drain current. When electric field increases, the avalanche multiplication becomes serious. Therefore, to suppress the kink effect, (i) improve the grain boundary quality (ii) enlarging the grain size (iii) let the grain boundary be away from the drain depletion region.



Chapter 4

Conclusion

DLC grain control technology

In this paper, we introduce a novel heat retaining material: diamond like carbon (DLC) to improve the laser crystallization process. The DLC film shows good optical absorbance over a wide wavelength. In the experiment, the DLC film is used as the heat retaining layer capped on the silicon film. Enhanced crystallization and locally-controlled grain structure are achieved around the DLC film. This lateral grain growth area can be defined by the DLC patterns and the grain size can achieve $1\mu m$ when the XeF excimer laser energy density is $600mJ/cm^2$. Along with the SEM images, micro-Raman is also used to analyze the crystallinity. It is found that when the laser energy density increases, the grain grows larger and the crystallinity of grain is also improved. The best Raman results show peak position as $516.25cm^{-1}$ and the FWHM as $4.9cm^{-1}$, which is comparable with other proposed H-REC results. Finally, thin buffer oxide is also used between the DLC film and the silicon film to avoid possible contamination from the DLC film. Similar grain growth results can be obtained and the crystallinity keeps good.

Analysis of grain affected kink effect

In Chapter 3, the grain structure influences on the kink effect of short-channel polysilicon TFTs are studied. It is well-known that the kink effect is mainly caused by the avalanche multiplication in depletion region near the drain. The avalanche

multiplication can be represented by the multiplication factor. When we extract the multiplication factor from device output characteristics, it is found that the multiplication factor is strongly affected by two factors: (i) grain boundary barrier height (E_B) and (ii) grain size (L_G). We found the grain boundary barrier height and also the multiplication factor decreases almost simultaneously as the gate voltage increases. It had been proposed theoretically that when the grain barrier height increases, the local high electric field caused by grain boundary barrier height is enlarged and the avalanche multiplication becomes more serious. In our study, we firstly observe this phenomenon from the experimental data. Moreover, the dependence of multiplication factor on the grain size is also clearly observed. When the grain size increases, the local grain boundary electric field is reduced and the multiplication factor also becomes smaller. Finally the dependence of lateral electric field on the multiplication factor is also confirmed by applying different drain bias. The behavior of the multiplication factor follow typical lucky-electron model under large drain bias.

Since the laser process can influence the grain boundary properties. Controlling the crystallization mechanism in super lateral growth regime can suppress the kink effect because both the grain size is enlarged and the boundary properties are improved. Different laser technology (excimer laser annealing and solid state laser annealing) are also used to fabricate devices with different film qualities. It is found that even having similar grain size, ELA-annealed films have larger grain boundary barrier than the SSL-annealed ones. This is consistent with the observed short channel performance in these devices. That is: Devices using ELA annealing process have more serious kink effect than devices using SLS annealing process even when the grain size is almost identical in all the devices. It is concluded that using SSL technology can suppress the kink effect. Developing the grain enlarge technology

such as using the DLC heat retaining layer is also a plausible solution to eliminate the kink effect.

